Electron Beam Evaporated TiO2 Layer for High Efficiency Planar Perovskite Solar Cells on Flexible Polyethylene Terephthalate Substrates

Journal of
Materials Chemistry A

Accepted Manuscript

This article can be cited before page numbers have been issued, to do this please use: W. Qiu, U. W. Paetzold, R. Gehlhaar, V. Smirnov, H. Boyen, J. G. Tait, B. Conings, W. Zhang, C. Nielsen, I. Mcculloch, L. Froyen, P. Heremans and D. Cheyns, *J. Mater. Chem. A*, 2015, DOI: 10.1039/C5TA07515G.

ROYAL SOCIETY OF CHEMISTRY

www.rsc.org/materialsA

View Article Online
DOI: 10.1039/C5TA07515G

Electron Beam Evaporated TiO_2 Layer for High Efficiency Planar Perovskite Solar Cells on Flexible Polyethylene Terephthalate Substrates

*Weiming Qiu [1,2 *], Ulrich W. Paetzold [1,4], Robert Gehlhaar [1], Vladimir Smirnov [4], Hans-Gerd Boyen [7], Jeffrey G. Tait [1], Bert Conings [7], Weimin Zhang [5], Christian B. Nielsen [5], Iain McCulloch [6], Ludo Froyen [2], Paul Heremans [1,3 *], David Cheyns[1]*

[1] Imec, Kapeldreef 75, 3001, Heverlee, Belgium

[2] MTM, KU Leuven, 3001, Heverlee, Belgium

[3] ESAT, KU Leuven, 3001, Heverlee, Belgium

[4] IEK5-Photovoltaik, Forschungszentrum Juelich GmbH, D-52425, Germany

[5] Department of Chemistry and Centre for Plastic Electronics, Imperial College London, SW7 2AZ, UK

[6] Physical Sciences and Engineering Division, King Abdullah University of Science and Technology (KAUST), Thuwal 23955-6900 , Saudi Arabia

[7] Institute for Materials Research, University of Hasselt, 3590, Belgium

[*] Corresponding Authors: Weiming.Qiu@imec.be; Paul.Heremans@imec.be

View Article Online
DOI: 10.1039/C5TA07515G

ABSTRACT: The TiO_2 layer made by electron beam (e-beam) induced evaporation is demonstrated as electron transport layer (ETL) in high efficiency planar junction perovskite solar cells. The temperature of the substrate and the thickness of the TiO_2 layer can be easily controlled with this e-beam induced evaporation method, which enables the usage of different types of substrates. Here, Perovskite solar cells based on $CH_3NH_3PbI_{3-x}Cl_x$ achieve power conversion efficiencies of 14.6% on glass and 13.5% on flexible plastic substrates. The relationship between the TiO_2 layer thickness and the perovskite morphology is studied with scanning electron microscope (SEM), atomic force microscope (AFM), and X-ray photoelectron spectroscopy (XPS). Our results indicate that pinholes in thin TiO_2 layer lead to pinholes in the perovskite layer. By optimizing the TiO_2 thickness, perovskite layers with substantially increased surface coverage and reduced pinhole areas are fabricated, increasing overall device performance.

KEYWORDS: perovskite solar cell; $CH_3NH_3PbI_{3-x}Cl_x$; electron beam evaporation; TiO_2; flexible substrates

GRAPHICAL ABSTRACT:

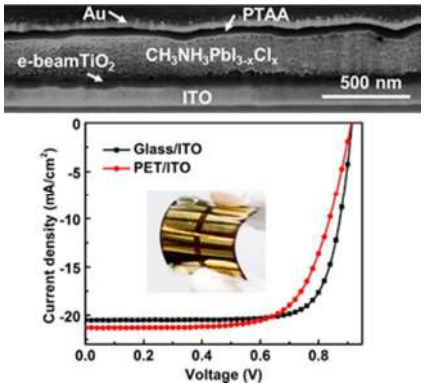

View Article Online
DOI: 10.1039/C5TA07515G

Introduction

Organometallic halide perovskite solar cells have attracted tremendous interest from both academia and industry. Within only a few years, an unprecedented certified power conversion efficiency (PCE) of 20.1% has been achieved for perovskite solar cells,[1] which makes it one of the most promising thin film photovoltaic technologies.[2,3] To date, most research groups report high efficiency perovskite solar cells employing a sol-gel or spray pyrolysis synthesized TiO_2 compact ETL that needs to be annealed at very high temperatures (500 °C).[4–10] The preparation of these sol-gel based TiO_2 layers is, however, typically complicated and incompatible with the thermal budget of flexible plastic substrates.[11]

Efforts have been made to develop low temperature alternatives to high temperature sol-gel based TiO_2 ETLs. For example, sol-gel prepared TiO_2 nanoparticles have been developed as a replacement, reducing annealing temperatures to 150 °C.[12,13] However, residual organic additives remain in these low temperature TiO_2 layers.[13] Moreover, 150 °C is still close to the maximum processing temperature for cheap plastic substrates such as polyethylene terephthalate (PET). Atomic layer deposition (ALD) is another promising alternative to get low temperature TiO_2 layers, but the PCE values of perovskite solar cells with ALD TiO_2 still needs to be improved.[14–17] Consequently, the development of high quality TiO_2 layers processed at low temperature is being ardently pursued.

The relatively low processing temperatures needed to form the perovskite crystal structure enables the use of organometallic halide perovskite in flexible thin film solar cells.[14] Yet, there

View Article Online
DOI: 10.1039/C5TA07515G

are few reports of flexible perovskite solar cells. Limited by the poor alternatives for the high temperature TiO_2 ETL in the n-i-p structure, most flexible perovskite solar cells are based on a p-i-n structure with poly(3,4-ethylenedioxythiophene): polystyrene sulfonate (PEDOT:PSS) as the hole transport layer on indium tin oxide (ITO) coated substrates.[18–21] However, PEDOT:PSS has proven detrimental to device stability in organic solar cells, due to its acidic and hygroscopic nature.[22] To the best of our knowledge, solution processed ZnO nanoparticles and ALD synthesized TiO_2 layers have been implemented in flexible perovskite solar cells with a n-i-p structure on flexible substrates, with the highest efficiencies of approximately 12%.[14,15,23,24] More recently, a photonic curing technique was also used to achieve TiO_2 layers at low processing temperatures on PET substrates, resulting in devices with PCE of only 8.1%.[25]

In this work, TiO_2 deposited by e-beam induced evaporation is examined as a compact ETL for perovskite solar cells. With this method, both layer thickness and substrate temperature can be controlled. Deposited with neither additives nor annealing steps, the e-beam evaporated TiO_2 can be used as prepared. Device efficiencies reach 14.6% with such TiO_2 ETL and $CH_3NH_3PbI_{3-x}Cl_x$ perovskite photoactive layer. Moreover, we demonstrate flexible perovskite solar cells with PCE values of 13.5% on PET substrates using our e-beam evaporated TiO_2 ETL, which are amongst the highest values for flexible perovskite solar cells.

Results and discussions

The optical properties of the e-beam TiO_2 layer were evaluated before making devices. Fig. 1a shows the results of refractive index (n) and extinction coefficient (k) measured by variable angle

View Article Online
DOI: 10.1039/C5TA07515G

spectroscopic ellipsometry. The e-beam TiO_2 layer is highly transparent in visible to near infrared wavelengths, which makes it a good candidate as ETL in thin-film photovoltaics. The crystallinity of the e-beam TiO_2 layer was checked with X-ray diffraction (XRD) and no diffraction peak is detected, indicating its amorphous nature (Fig. 1b).

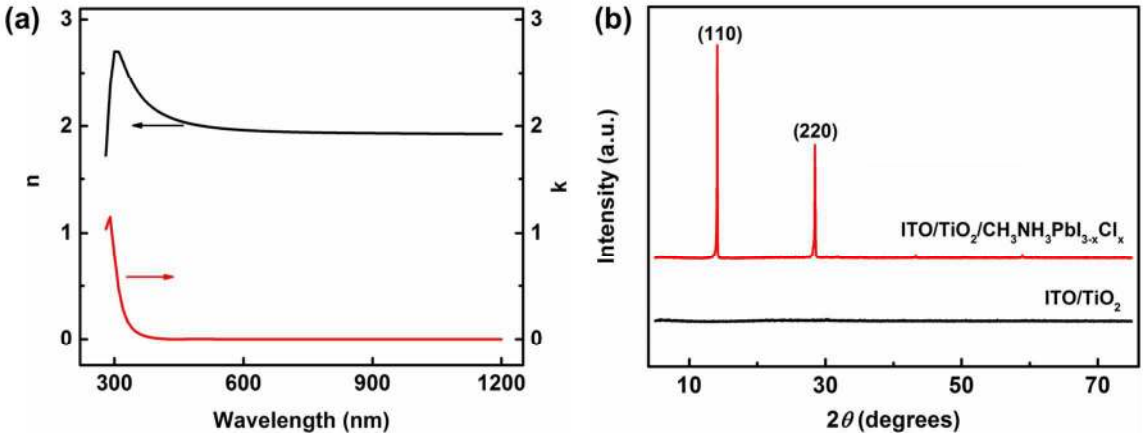

Fig. 1 (a) The refractive index (n) and extinction coefficient (k) of the e-beam TiO_2 layer. (b) The XRD patterns of ITO/e-beam TiO_2 and ITO/e-beam TiO_2/ $CH_3NH_3PbI_{3-x}Cl_x$.

To fabricate the perovskite solar cell, typically a 300 nm thick $CH_3NH_3PbI_{3-x}Cl_x$ perovskite layer was made on 60 nm thick e-beam TiO_2 layer. After annealing, the $CH_3NH_3PbI_{3-x}Cl_x$ shows a highly crystalline perovskite structure,[26] as indicated by XRD pattern (Fig. 1b). To complete the device, doped poly(triaryl amine) PTAA was used as hole transport layer and Au was used as anode. Therefore, our devices have an architecture of ITO/TiO_2 /$CH_3NH_3PbI_{3-x}Cl_x$/PTAA/Au, as indicated by the cross-sectional SEM image of our typical device on glass substrate (Fig. 2a).

View Article Online
DOI: 10.1039/C5TA07515G

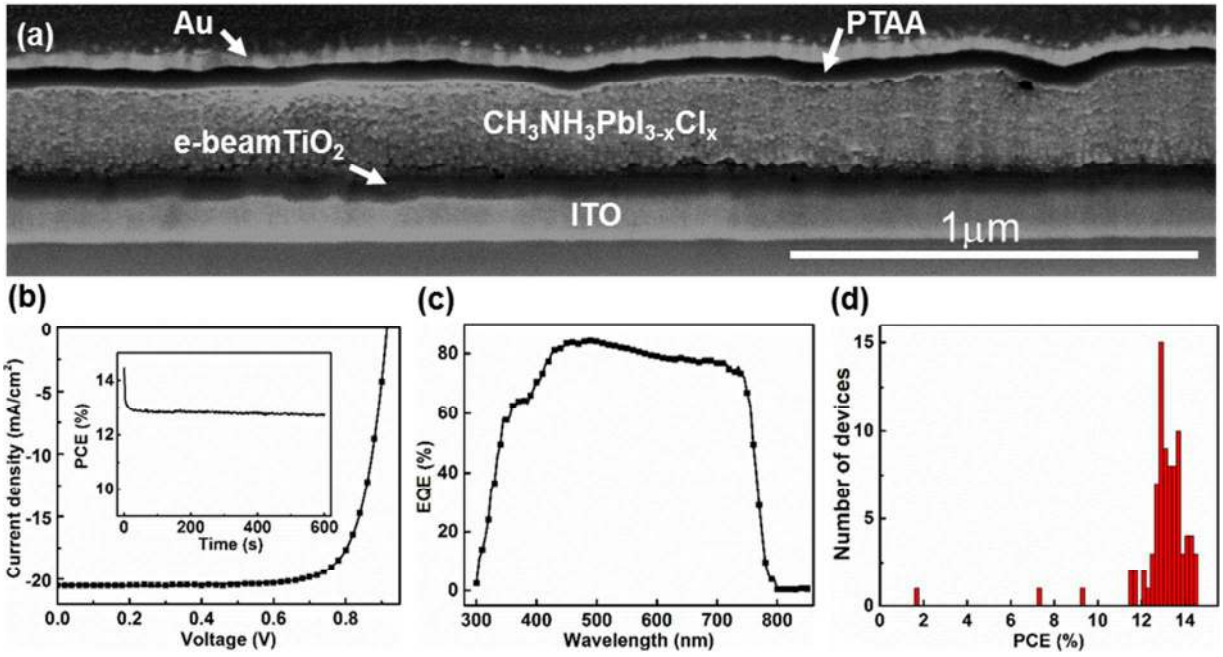

Fig. 2 (a) A cross-sectional SEM image of a planar $CH_3NH_{3-x}Cl_x$ perovskite device, prepared with a focused ion beam. (b) The current density-voltage curve of the device with the highest efficiency. The inset presents the quasi-steady state efficiency measured at the maximum power point voltage (0.72 V) over time. (c) The EQE of the device with the highest efficiency, peaking at 85%, and giving an integrated Jsc in AM1.5G of (19.5 mA/cm2). (d) A histogram of the efficiency values for 84 devices, with a mean efficiency of 13.2 ± 0.5%.

The current density-voltage (*J-V*) plot of the highest efficiency device on a rigid glass substrate, measured from forward bias to reverse bias using a measurement speed of 1 V/s, is shown in Fig. 2b. The device demonstrates an open-circuit voltage (V_{oc}) of 0.91 V, a short-circuit current density (J_{sc}) of 20.5 mA/cm^2, and a fill factor (*FF*) of 78%, giving a PCE of 14.6%. The J_{sc} calculated from the corresponding EQE curve is 19.5 mA/cm^2, within 5% mismatch compared to the value measured from the *J-V* scan (Fig. 2c). The quasi-steady state efficiency of the device is

View Article Online
DOI: 10.1039/C5TA07515G

measured by operating the device at the maximum power point voltage (0.72 V) as obtained from the *J-V* scan (inset, Fig. 2b**)**. A rapid drop of the efficiency from 14.6% to 13% is observed within the first 15 seconds, likely due to the hysteresis effects observed in perovskite devices.[27] The efficiency gradually stabilizes and reaches 12.8% after 10 minutes of operation. The histogram of the initial efficiency values from 84 devices displays a high yield (96%) of working devices (PCE > 11%) with a mean efficiency of 13.2 ± 0.5% (Fig. 2d), indicating high efficiency perovskite solar cells are achievable on amorphous TiO_2 layers.

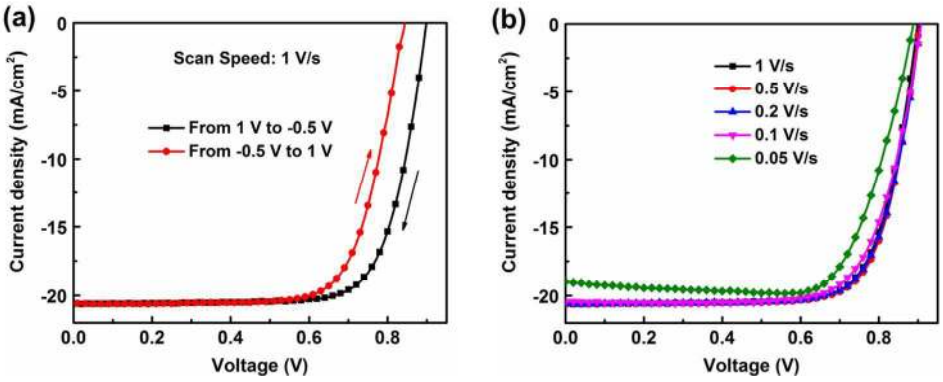

Fig.3 *J-V* curves of the device made on 60 nm e-beam TiO_2: (a) measured from different scan directions; (b) Measured from different scan speeds. The detailed photovoltaic parameters are shown in Table S1.

To have more evaluation of the hysteresis of the devices made on e-beam TiO_2, *J-V* scan from different directions are shown in Fig. 3a. The reverse scan from 1 V to -0.5 V gives higher efficiency of 13.9% than the efficiency (12.6%) of the forward scan from -0.5 V to 1 V, which is mainly due to the higher V_{oc} and FF. Moreover, the same device was also measured with

View Article Online
DOI: 10.1039/C5TA07515G

different *J-V* scan speed. From Fig. 3b, we can find the *J-V* curve and efficiency do not change much when the scan speed reduced from 1 V/s to 0.1 V/s. However, if the scan speed is too slow, it starts to have significant effects and gives abnormal *J-V* curves. In this case, it will be difficult to extract the real photovoltaic parameters from the *J-V* curves. Therefore, we suggest to use a relative high scan speed to find out the maximum power point and measure the stabilized efficiency around the maximum power point, in order to have a better evaluation of the device performance.

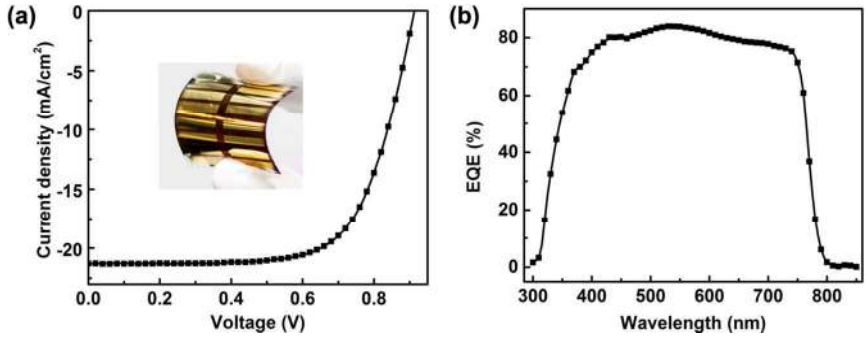

Fig. 3 (a) A *J-V* plot, and (b) the corresponding EQE curve of the highest efficiency (13.5%) device fabricated on a flexible PET substrate. The inset of (a) shows a digital photograph of the devices.

To verify the low temperature process of the e-beam TiO_2, an irreversible temperature sensor strip was taped on the sample holder to detect the temperature of the samples during the e-beam induced evaporation. As is shown in Fig. S1, no change is observed on the temperature sensor, indicating that the temperature of the samples never exceeded the lowest detectable temperature (77℃) for this type of temperature sensor. Such a low temperature budget of the whole stack

View Article Online
DOI: 10.1039/C5TA07515G

(≤100 °C) enables the use of flexible plastic substrates. Perovskite solar cells with e-beam TiO_2 reach high efficiencies of 13.5% on ITO coated PET substrates. The *J-V* plots measured on the highest efficiency device show V_{oc} of 0.91 V, J_{sc} of 21.3 mA/cm^2, and FF of 69% (Fig. 4a**)**. The J_{sc} calculated from the corresponding EQE curve at AM1.5G conditions is 19.9 mA/cm^2 (Fig. 4b). Moreover, compared to the highest performing device on a glass substrate, the highest performing flexible device shows only a relatively lower FF, while the V_{oc} and J_{sc} are similar. This lower FF may be partially resulted from the higher sheet resistance of the ITO on the PET substrate (35 Ω/square), compared to that on glass substrate (15 Ω/square). Therefore, e-beam evaporated TiO_2 is a good candidate for ETL that suits both glass and plastic substrates.

Table 1. Photovoltaic performance values of the perovskite devices fabricated with increasing e-beam TiO_2 layer thickness.

TiO_2 Thickness (nm)	J_{sc} (mA/cm^2)	V_{oc} (V)	FF (%)	PCE (%)
15	19.6 ± 0.3	0.78 ± 0.01	60 ± 2	9.0 ± 0.5
30	20.1 ± 0.1	0.88 ± 0.01	71 ± 2	12.4 ± 0.4
45	20.5 ± 0.2	0.90 ± 0.01	72 ± 2	13.1 ± 0.5
60	20.5 ± 0.3	0.89 ± 0.01	73 ± 2	13.4 ± 0.6
80	20.0 ± 0.2	0.83 ± 0.03	74 ± 2	12.4 ± 0.7

The above devices are all made on e-beam TiO_2 layers with an optimized thickness of 60 nm. It is found that the thickness of the TiO_2 layer has a crucial influence on the devices performance (Table 1). Increasing the TiO_2 layer thickness from 15 nm to 45 nm leads to a significant improvement of all the photovoltaic parameters. An additional increase in FF occurs for even

View Article Online
DOI: 10.1039/C5TA07515G

thicker TiO_2 layers (60 nm). No further improvement in device performance is observed for thicknesses above 60 nm. Top-view SEM of perovskite layers on e-beam TiO_2 indicate that the size of pinholes in the perovskite dramatically decreases with an increased TiO_2 layer thickness (Fig. 5). The area coverage loss from pinholes in the perovskite layer is 3.4% for 15 nm and 0.5% for 30 nm thick TiO_2 layers. Nearly negligible area losses are found for TiO_2 layer thicknesses of 45 and 60 nm. This increase in active area can result in an increased light absorption as well as reduced shunt currents, leading to an improvement of all photovoltaic parameters.

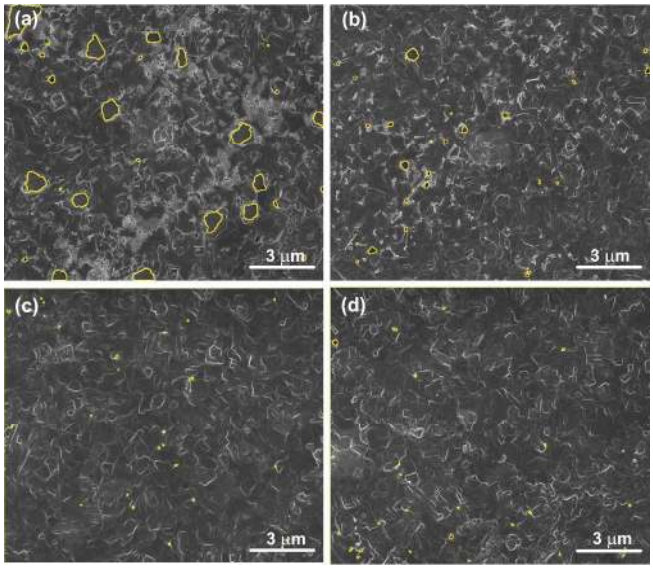

Fig. 5 Top-view SEM images of the perovskite ($CH_3NHPbI_{3-x}Cl_x$) layers deposited on e-beam TiO_2 layers with thicknesses of: (a) 15 nm, (b) 30 nm, (c) 45 nm, and (d) 60 nm. The percentage of calculated pinhole area are 3.4%, 0.5%, 0.09%, and 0.06% from (a) to (d), respectively.

While similar observations that thicker TiO_2 layer gives better morphology of the perovskite layer have been reported by others, the origin remains poorly understood.[28,29] Speculatively, Snaith *et al* suggested that a thicker TiO_2 layer was able to electrostatically stabilize the

View Article Online
DOI: 10.1039/C5TA07515G

perovskite formation near the surface.[28] We propose that the roughness and pinhole density in these perovskite films is related to the pinhole concentration in the TiO_2 layer. A greater density of pinholes in thinner TiO_2 layers exposes the perovskite precursor solution to bare ITO. The spin coating of precursors and formation of perovskite directly on ITO leads to extremely rough films with copious numbers of pinholes, demonstrating the apparent high stress interface between ITO and $CH_3NH_3PbI_{3-x}Cl_x$.

AFM and XPS on TiO_2 layers with different thickness confirm the existence of pin-holes in thinner TiO_2 layers. The AFM images in Fig. 6 indicate similar surface topography and platelet sizes for each thickness of TiO_2, and only a slight change of the root-mean-square (RMS) roughness from 4.21 nm to 3.81 nm with increasing TiO_2 thickness. Also, each TiO_2 layer thickness has a similar peak-to-valley depth of approximately 30 nm. With the peak-to-valley depth of similar magnitude to the layer thickness, it is probable that some of the valleys measured in the 15 and 30 nm thick TiO_2 layer are ITO surfaces. The thicker TiO_2 layers likely reduce the chance of exposing the underlying ITO surface.

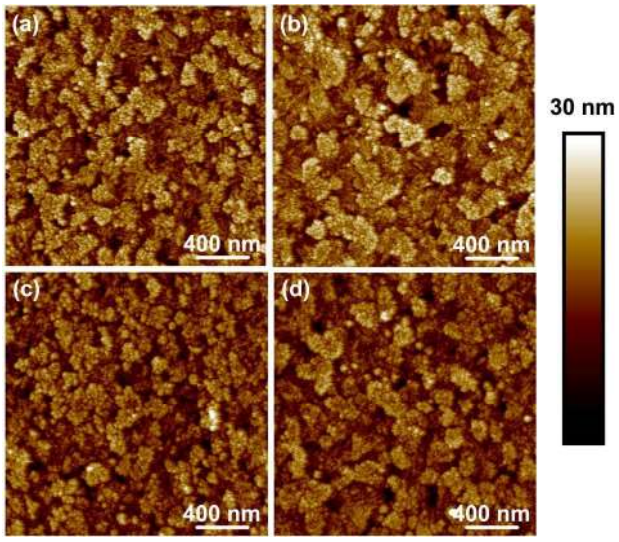

View Article Online
DOI: 10.1039/C5TA07515G

Fig. 6. AFM images of e-beam deposited TiO_2 layers with thicknesses: (a) 15 nm, (b) 30 nm, (c) 45 nm, and (d) 60 nm.

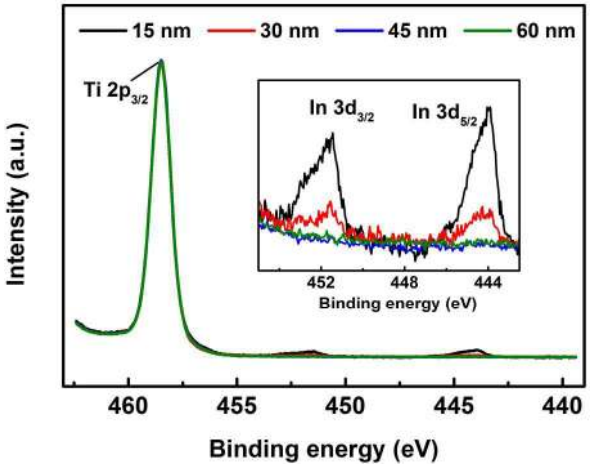

Fig. 7 Each layer thickness (15, 30, 45, and 60 nm) of e-beam TiO_2 show similar XPS spectra for the Ti $2p_{3/2}$ peak. The zoomed-in inset shows the In $3d_{3/2}$ and $3d_{5/2}$ peaks decreasing with layer thickness from 15 to 60 nm. Neither of the two In peaks are discernable for the 45 and 60 nm thicknesses.

XPS measurement further substantiates the exposure of ITO at the surface of samples with thin TiO_2 layers (Fig.7). All samples have the same shape of the spectra and binding energy (458.5 eV) for Ti $2p_{3/2}$ XPS peak, which can be attributed to TiO_2.[13] This shape in energy signifies that there is no difference in the chemical composition for the different TiO_2 thicknesses. Thus, similar surface properties, e.g. the surface energy, are expected. However, signals of In 3d can be found in the XPS spectrum obtained from the samples with 15 and 30 nm thickness of TiO_2 on ITO. The intensity of the In 3d peaks decreases with increasing TiO_2 thickness until finally they are undetectable for layer thickness above 45 nm. Since XPS is surface sensitive to

View Article Online
DOI: 10.1039/C5TA07515G

approximately 5 nm in depth, the observation of the In 3d signals clearly indicate the existence of pinholes in thin TiO_2 layers, coinciding with the results from AFM. Since the TiO_2 layers with identical chemical composition are evaporated, all evidence points to pinholes in the thin TiO_2 layers accounting for the poor morphology of the subsequently deposited perovskite layers, and thus lead to increasing device performance with increasing TiO_2 thickness.

Conclusions

In summary, a low temperature e-beam deposited TiO_2 layer is examined as an alternative to the archetypal, high temperature sol-gel prepared TiO_2 for $CH_3NH_3PbI_{3-x}Cl_x$ based perovskite solar cells. Planar perovskite solar cells are demonstrated on both glass and PET substrates, achieving efficiencies of 14.6% and 13.5%, respectively. The thickness of the e-beam TiO_2 layer plays a critical role in determining the morphology of the subsequently deposited perovskite layer. We propose that the pinholes in thin TiO_2 layers expose the underlying ITO, and lead to pinholes in the perovskite layer. Thus, for complete coverage of perovskite and high performance, it is imperative that the TiO_2 layer be sufficiently thick to fully cover the ITO. The e-beam induced TiO_2 deposition enables processing of low temperature ETLs for n-i-p structure perovskite devices with high efficiency and freedom of substrate choice, taking the field another step closer to industrial scale production.

Experimental section

Fabrication of perovskite solar cells

View Article Online
DOI: 10.1039/C5TA07515G

The glass substrates with patterned ITO electrodes were purchased from Colorado Concept Coatings. ITO electrodes on PET substrate were deposited using a low temperature radio-frequency magnetron sputtering of In_2O_3:SnO_2 (95/5wt.%) according to the procedures reported previously.[30] The ITO coated glass and PET substrates were first cleaned with ultrasonic baths of detergent, deionized water, acetone, and iso-propanol for 10 minutes each. The substrates were then transferred into an evaporation system (Angstrom Engineering) equipped with an electron beam source. The TiO_2 pellets (Prof. Feierabend GmbH) were evaporated at a rate of 2 Å/s onto ITO substrates using a partial O_2 pressure of 1.7×10^{-4} Torr during the deposition to maintain the stoichiometry of the film. The 40 wt.% $CH_3NH_3PbI_{3-x}Cl_x$ precursor solution, containing $PbCl_2$ (Sigma-Adrich) and CH_3NH_3I (Lumtec) with a molar ratio of 1:3 in N,N-dimethylformamide (DMF), was spin coated at 4000 rpm for 60 s onto the TiO_2 layer. The obtained films were annealed on a hot plate at 100 °C for 1 h to form the perovskite structure. After that, 10 mg/ml PTAA solution (15 mg in 1.5 ml chlorobenzene) doped with 15 µl lithium bis(trifluoromethanesulfonyl) imide (170 mg/ml in acetonitrile) and 7.5 µl 4-tert-butylpyridine was spin coated onto the perovskite layers. All of the spin coating processes mentioned above were performed in N_2 filled glove box. The PTAA material (M_n = 45500 g/mol and M_w = 96400 g/mol) was synthesized as reported.[31] The devices were completed by depositing an 80 nm Au layer onto the PTAA through shadow masks, defining twelve devices on one substrate, each with an active area of 0.13 cm^2.

Instruments and characterizations

Photovoltaic characteristics of the devices were measured under a nitrogen atmosphere using a Keithley 2602A Source-Measure Unit and an Abet solar simulator with 100 mW/cm^2 simulated

View Article Online
DOI: 10.1039/C5TA07515G

AM1.5G illumination, calibrated with an KG5 band pass equipped ISE Fraunhofer certified Si photodiode. The devices were measured from forward to reverse bias with a scan speed of 1 V/s. The quasi-steady state current density was measured by operating the devices at the maximum power voltage that was found in the initial current density-voltage scan measurements. The quasi-steady state efficiencies were calculated by multiplying the quasi-steady state current density and the operating voltage. The EQE was measured with a photospectrometer setup (Bentham PVE300) by illuminating the solar cell with a modulated monochromatic light (Xe and quartz halogen lamps). The complex index of refraction was measured by variable angle spectroscopic ellipsommetry (VASE, ges5, sopra). The XRD pattern was recorded on a PANalyticalX'Pert Pro Materials Research Diffractometer using Cu Kα radiation. The top-view SEM images were obtained from FEI Nova 200 scanning electron microscope. AFM images were obtained from Bruker dimension edge system in peak-force tapping mode. XPS experiments were performed on a Physical Electronics (PHI) 5600LS electron spectrometer, equipped with a small-spot X-ray source providing monochromatic Al Kα photons (1486.6 eV) with resolutions of <0.4 and 0.04 eV, respectively. The binding energy scale was calibrated by means of an independent Au reference sample, setting the Au $4f_{7/2}$ core-level position to 84.00 eV.

Acknowledgement

The authors would like to acknowledge Kjell Cnops for the XRD measurement, Elmar Neumann for the cross-sectional sample preparation using FIB, and Ziyang Liu for taking the top-view SEM images. This research has received (partial) funding from the Flemish Government – Department of Economics, Science and Innovation. J.G. Tait would like to acknowledge partial

View Article Online
DOI: 10.1039/C5TA07515G

funding by the Natural Science and Engineering Council of Canada. U. W. Paetzold would like to thank the financial support from the PostDoc Program of the German Academic Exchange Program (DAAD).

References

1 M. A. Green, K. Emery, Y. Hishikawa, W. Warta, E. D. Dunlop, *Prog. Photovoltaics Res. Appl.*, 2015, **23**, 1.

2 M. Grätzel, *Nat. Mater.*, 2014, **13**, 838.

3 M. A. Green, A. Ho-Baillie, H. J. Snaith, *Nat. Photonics*, 2014, **8**, 506.

4 K. Yan, M. Long, T. Zhang, Z. Wei, H. Chen, S. Yang, J. Xu, *J. Am. Chem. Soc.*, 2015, **137**, 4460.

5 W. Zhang, M. Saliba, D. T. Moore, S. K. Pathak, M. T. Hörantner, T. Stergiopoulos, S. D. Stranks, G. E. Eperon, J. A. Alexander-Webber, A. Abate, A. Sadhanala, S. Yao, Y. Chen, R. H. Friend, L. A. Estroff, U. Wiesner, H. J. Snaith, *Nat. Commun.,* 2015, **6**, 6142.

6 N. J. Jeon, J. H. Noh, Y. C. Kim, W. S. Yang, S. Ryu, S. Il Seok, *Nat. Mater.,* 2014, **13**, 1.

7 N. J. Jeon, J. H. Noh, W. S. Yang, Y. C. Kim, S. Ryu, J. Seo, S. Il Seok, *Nature*, 2015, **517**,476.

8 J.-H. Im, I.-H. Jang, N. Pellet, M. Grätzel, N.-G. Park, *Nat. Nanotechnol.*, 2014, **9**, 927.

9 J.-W. Lee, D.-J. Seol, A.-N. Cho, N.-G. Park, *Adv. Mater.*, 2014, **26**, 4991.

View Article Online
DOI: 10.1039/C5TA07515G

10 J. Burschka, N. Pellet, S.-J. Moon, R. Humphry-Baker, P. Gao, M. K. Nazeeruddin, M. Grätzel, *Nature*, 2013, **499**, 316.

11 Q. Hu, J. Wu, C. Jiang, T. Liu, X. Que, R. Zhu, Q. Gong, *ACS Nano*, 2014, **8**, 10161.

12 H. Zhou, Q. Chen, G. Li, S. Luo, T. -b. Song, H.-S. Duan, Z. Hong, J. You, Y. Liu, Y. Yang, *Science*, 2014, **345**, 542.

13 B. Conings, L. Baeten, T. Jacobs, R. Dera, J. D'Haen, J. Manca, H.-G. Boyen, *APL Mater.*, 2014, **2**, 081505.

14 B.-J. Kim, dong H. Kim, Y.-Y. Lee, H.-W. Shin, G. S. Han, J. S. Hong, K. Mahmood, T. Ahn, Y.-C. Joo, K. S. Hong, N.-G. Park, S. Lee, H. S. Jung, *Energy Environ. Sci.,* 2015, **8**, 916.

15 F. Di Giacomo, V. Zardetto, A. D'Epifanio, S. Pescetelli, F. Matteocci, S. Razza, A. Di Carlo, S. Licoccia, W. M. M. Kessels, M. Creatore, T. M. Brown, *Adv. Energy Mater.*, 2015, doi: 10.1002/aenm.201401808 .

16 A. K. Chandiran, A. Yella, M. T. Mayer, P. Gao, M. K. Nazeeruddin, M. Grätzel, *Adv. Mater*., 2014, **26**, 4309.

17 Y. Wu, X. Yang, H. Chen, K. Zhang, C. Qin, J. Liu, W. Peng, A. Islam, E. Bi, F. Ye, M. Yin, P. Zhang, L. Han, *Appl. Phys. Express*, 2014, **7**, 52301.

18 P. Docampo, J. M. Ball, M. Darwich, G. E. Eperon, H. J. Snaith, *Nat. Commun*., 2013, **4**, 2761.

19 J. W. Jung, S. T. Williams, A. K.-Y. Jen, *RSC Adv.*, 2014, **4**, 62971.

20 Y. Yang, J. You, Z. Hong, Q. Chen, M. Cai, T. Bin Song, C. C. Chen, S. Lu, Y. Liu, H. Zhou, *ACS Nano,* 2014, **8**, 1674.

View Article Online
DOI: 10.1039/C5TA07515G

21 Z. Yang, C.-C. Chueh, F. Zuo, J. H. Kim, P.-W. Liang, A. K.-Y. Jen, *Adv. Energy Mater.*, 2015, doi: 10.1002/aenm.201500328.

22 E. Voroshazi, B. Verreet, A. Buri, R. Müller, D. Di Nuzzo, P. Heremans, *Org. Electron.,* 2011, **12**, 736.

23 M. H. Kumar, N. Yantara, S. Dharani, M. Graetzel, S. Mhaisalkar, P. P. Boix, N. Mathews, *Chem. Commun.,* 2013, **49**, 11089.

24 D. Liu, T. L. Kelly, *Nat. Photonics*, 2013, **8**, 133.

25 S. Das, B. Yang, G. Gu, P. C. Joshi, I. N. Ivanov, C. M. Rouleau, T. Aytug, D. B. Geohegan, K. Xiao, *ACS Photonics,* 2015, **2**, 680.

26 M. Liu, M. B. Johnston, H. J. Snaith, *Nature*, 2013, **501**, 395.

27 H. J. Snaith, A. Abate, J. M. Ball, G. E. Eperon, T. Leijtens, N. K. Noel, S. D. Stranks, J. T. W. Wang, K. Wojciechowski, W. Zhang, *J. Phys. Chem. Lett.*, 2014, **5**, 1511.

28 G. E. Eperon, V. M. Burlakov, P. Docampo, A. Goriely, H. J. Snaith, *Adv. Funct. Mater.*, 2014, **24**, 151.

29 Z. Yuan, Z. Wu, S. Bai, Z. Xia, W. Xu, T. Song, H. Wu, L. Xu, J. Si, Y. Jin, B. Sun, *Adv. Energy Mater*., 2015, doi:10.1002/aenm.201500038.

30 K. Wilken, U. W. Paetzold, M. Meier, N. Prager, M. Fahland, F. Finger, and V. Smirnov, *Phys. Status Solidi RRL*, 2015, **9**, 215.

31 W. Zhang, J. Smith, R. Hamilton, M. Heeney, J. Kirkpatrick, K. Song, S. E. Watkins, T. Anthopoulos, I. McCulloch, *J. Am. Chem. Soc.*, 2009, **131**, 10814.